Title: Stage-specific disruption of X chromosome expression during spermatogenesis in sterile house mouse hybrids

Authors: Erica L. Larson[1], Emily E. K. Kopania[2], Kelsie E. Hunnicutt[1], Dan Vanderpool[2], Sara Keeble[2] and Jeffrey M. Good[2]

[1] Department of Biological Sciences, University of Denver, Denver, CO 80208

[2] Division of Biological Sciences, University of Montana, Missoula, MT 59812

ORCID ID: 0000-0003-3006-645X (ELL)

ORCID ID: 0000-0002-2710-2491 (EEKK)

ORCID ID: 0000-0002-9674-0630 (KEH)

ORCID ID: 0000-0002-6856-5636 (DV)

ORCID ID: 0000-0003-0707-5374 (JMG)

Data Availability: The data reported in this paper are available through the National Center for Biotechnology Information Sequence Read Archive under accession numbers PRJNA296926 (*domesticus* and *musculus* RNAseq data), PRJNA352861 (F1 hybrid RNAseq data), PRJNA732719 (lab strain whole genome sequence data). *Prdm9* sequences were deposited in Genbank under accession numbers MZ733983-MZ733986. Male reproductive phenotype data are available in Table S1.

Running Title: Disruption of X chromosome expression in sterile hybrids

Keywords: speciation, genomic conflict, hybrid male sterility, testis expression, sex chromosomes, PRDM9

Corresponding Authors:

Erica L. Larson

Department of Biological Sciences

University of Denver

Denver, CO 80208

Phone: (303) 871 - 3694

Email: erica.larson@du.edu

Jeffrey M. Good

Division of Biological Sciences

University of Montana

Missoula, MT 59812

Phone: (406) 243 - 5122

Email: jeffrey.good@umontana.edu

ABSTRACT

Hybrid sterility is a complex phenotype that can result from the breakdown of spermatogenesis at multiple developmental stages. Here, we disentangle two proposed hybrid male sterility mechanisms in the house mice, *Mus musculus domesticus* and *M. m. musculus*, by comparing patterns of gene expression in sterile F1 hybrids from a reciprocal cross. We found that hybrid males from both cross directions showed disrupted X chromosome expression during prophase of meiosis I consistent with a loss of Meiotic Sex Chromosome Inactivation (MSCI) and *Prdm9*-associated sterility, but that the degree of disruption was greater in mice with an *M. m. musculus* X chromosome consistent with previous studies. During postmeiotic development, gene expression on the X chromosome was only disrupted in one cross direction, suggesting that misexpression at this later stage was genotype-specific and not a simple downstream consequence of MSCI disruption which was observed in both reciprocal crosses. Instead, disrupted postmeiotic expression may depend on the magnitude of earlier disrupted MSCI, or the disruption of particular X-linked genes or gene networks. Alternatively, only hybrids with a potential deficit of *Sly* copies, a Y-linked ampliconic gene family, showed overexpression in postmeiotic cells, consistent with a previously proposed model of antagonistic coevolution between the X and Y-linked ampliconic genes contributing to disrupted expression late in spermatogenesis. The relative contributions of these two regulatory mechanisms and their impact on sterility phenotypes awaits further study. Our results further support the hypothesis that X-linked hybrid sterility in house mice has a variable genetic basis, and that genotype-specific disruption of gene regulation contributes to overexpression of the X chromosome at different stages of development. Overall, these findings underscore the critical role of epigenetic regulation of the X chromosome during spermatogenesis and suggest that these processes are prone to disruption in hybrids.

INTRODUCTION

Hybrid sterility can result from the breakdown of gametogenesis at several developmental stages, from early divisions of mitotic cells, meiosis, to the differentiation of postmeiotic cells into mature gametes. After gamete production, hybrid fertility can also be reduced through mechanisms that impede fertilization, such as a failure of hybrid sperm to transfer or fertilize. In hybrid males, sterility is typically measured by quantitative traits such as testes weight and histology; sperm counts, motility, and morphology; and the ability to sire offspring. Often, these traits are correlated (White *et al.* 2011; Turner and Harr 2014; Larson *et al.* 2018b) and are evaluated as though they were a single phenotype, but that does not mean sterility arises from a single mechanism or genetic basis (Reed and Markow 2004; Campbell and Nachman 2014). To tease apart different mechanisms of hybrid sterility requires a developmental framework, where breakdown at different stages of spermatogenesis can be evaluated to understand, as a whole, the evolution of hybrid sterility (Larson *et al.* 2018a; Cutter and Bundus 2020).

Hybrid sterility is often a composite phenotype because it typically has a complex genetic basis that involves the negative epistatic interactions of multiple alleles, known as Dobzhansky-Muller Incompatibilities or DMIs (Dobzhansky 1937; Muller 1942, see also Bateson 1909). Incompatible alleles can be polymorphic or have modifiers that affect their expression (Cutter 2012), so that the extent of reproductive isolation varies among individuals within or between populations (Good *et al.* 2008b; Sweigart and Flagel 2015; Case *et al.* 2016; Mandeville *et al.* 2017; Bracewell *et al.* 2017; Zuellig and Sweigart 2018). DMIs can also evolve early in the divergence process (Coughlan and Matute 2020) and are expected to accumulate over time so that many different epistatic combinations of alleles may contribute to hybrid breakdown (Moyle and Nakazato 2010; Wang *et al.* 2013). Gene flow between populations can also lead to recombination of incompatible alleles (Bank *et al.* 2012; Lindtke and Buerkle 2015), which can further complicate patterns of population-level variation in DMIs (Larson *et al.* 2018b;

Meiklejohn *et al.* 2018). For all these reasons, careful laboratory dissection of sterility phenotypes remains a critical component of understanding the genetic basis of speciation.

Between subspecies of house mice, *Mus musculus domesticus* and *M. m. musculus* (hereafter *domesticus* and *musculus*), the evolution of hybrid sterility appears to be due to a combination of several genetic factors. These subspecies diverged ~350-500 mya (Geraldes *et al.* 2011; Duvaux *et al.* 2011; Phifer-Rixey *et al.* 2020) and have come into secondary contact in a long hybrid zone in central Europe (Macholán *et al.* 2012; Phifer-Rixey and Nachman 2015). Female hybrids are generally more fertile than males (but see Suzuki and Nachman 2015) and hybrid male fertility varies considerably in the hybrid zone (Turner *et al.* 2012). In crosses between *domesticus* females and *musculus* males, hybrid male sterility depends on which individual genotypes are sampled, while crosses between *musculus* females and *domesticus* males typically produce sterile hybrid males (Vanlerberghe *et al.* 1986; Alibert *et al.* 1997; Britton-Davidian *et al.* 2005; Vyskočilová *et al.* 2005; Good *et al.* 2008b; Turner *et al.* 2012).

There are many different autosomal regions that have been associated with hybrid sterility in house mice (*e.g.,* Oka *et al.* 2007; Good *et al.* 2008a; White *et al.* 2011; Turner *et al.* 2014; Turner and Harr 2014; Larson *et al.* 2018b; Schwahn *et al.* 2018; Morgan *et al.* 2020; Widmayer *et al.* 2020), but the primary genetic determinant of sterility in F1 hybrid males involves the rapid evolution of PRDM9 binding sites, the autosomal encoded protein that directs the location of recombination in mammals (Mihola *et al.* 2009; Mukaj *et al.* 2020). In F1 mouse hybrids, PRDM9 binds preferentially to ancestral binding sites, leading to the asymmetric formation of double strand breaks and autosomal asynapsis (Davies *et al.* 2016; Gregorova *et al.* 2018). When the number of asynapsed chromosomes in a cell reaches a threshold, it can trigger cell death and in the most severe cases, complete meiotic arrest (Bhattacharyya *et al.* 2013). *Prdm9*-associated sterility is polymorphic, with alternative 'fertile' *Prdm9* alleles (Flachs *et al.* 2012; Mukaj *et al.* 2020) and is further modulated by epistatic interactions with a locus on

the *musculus* X chromosome (*Hstx2,* Storchová *et al.* 2004; Bhattacharyya *et al.* 2014; Lustyk *et al.* 2019). A characteristic signal of *Prdm9*-associated sterility is the overexpression of the X chromosome during early meiosis I (Good *et al.* 2010; Bhattacharyya *et al.* 2013; Campbell *et al.* 2013; Turner *et al.* 2014; Larson *et al.* 2017), a developmental stage where the X chromosome would normally be transcriptionally inactive known as Meiotic Sex Chromosome Inactivation (MSCI, Turner 2015). Whether disrupted MSCI is a byproduct, or an integral part of *Prdm9*-associated sterility is still unclear (Forejt *et al.* 2021), but it is a distinct regulatory phenotype of hybrid sterility at this developmental stage.

Hybrid male sterility in house mice may also be influenced by interactions among three ampliconic sex-linked gene families expressed in postmeiotic cells, *Slx* and *Slxl1* (X chromosome) and *Sly* (Y chromosome, Ellis *et al.* 2011; Cocquet *et al.* 2012). SLY plays a central role in repressing the transcription of sex-linked genes, known as postmeiotic sex chromosome repression (PSCR), while SLX/SLXL1 counteract the repression of SLY by competing for binding access to SSTY1 at the promoter of thousands of postmeiotic genes (Moretti *et al.* 2020). *SLY* and *SLX/SLXL1* appear to compete through a copy-number arms race, with higher relative gene copies of *Sly* leading to the repression of other multicopy genes. Gene knockdowns of *Sly* (*i.e.*, *Sly*-deficient) result in the overexpression of the X chromosome and female-biased litters (Cocquet *et al.* 2009; Kruger *et al.* 2019), while knockdowns of *Slx*/*Slxl1* (*i.e.*, *Slx*-deficient) result in a slight underexpression of the X chromosome and male-biased litters (Cocquet *et al.* 2010, 2012; Kruger *et al.* 2019). These genes have undergone a massive co-amplification across different mouse lineages, leading to different copy numbers in *domesticus* and *musculus* (Ellis *et al.* 2011; Morgan and Pardo-Manuel de Villena 2017). As a result, F1 hybrids between *musculus* females and *domesticus* males potentially have a deficit of *Sly* gene copies, while hybrids from the reciprocal cross have a deficit of *Slx/Slxl1* gene copies (Good 2012). We previously demonstrated that the X chromosome in postmeiotic cells is

overexpressed in *Sly*-deficient hybrids, consistent with *Sly*/*Slx*-associated sterility (Larson *et al.* 2017). We also observed overexpression in *Sly*-deficient hybrids of an ampliconic autosomal gene family, *α-takusan*, that is regulated by *SLY* (Moretti *et al.* 2017) and a slight underexpression of the X chromosome in *Slx*-deficient hybrids, consistent with *Sly* repression (Kruger *et al.* 2019). These results support a model of postmeiotic disruption of X chromosome expression and *Sly*/*Slx*-associated sterility.

Incompatibilities at each of these stages may produce similar sterility phenotypes, such as low testes weight and abnormal sperm morphology, making it difficult to tease apart their contribution to overall hybrid sterility and the maintenance of the house mouse hybrid zone. The disrupted expression of the X chromosome at different developmental stages suggests that hybrid sterility in these mice is a composite of multiple regulatory mechanisms (Larson *et al.* 2017). However, because both *Prdm9* and *Sly*/*Slx* associated sterility are often asymmetric and depend on interactions with the *M. m. musculus* X chromosome it is possible that postmeiotic disruption of the X chromosome observed in some crosses is simply a downstream effect of disrupted MSCI and a cascade of disrupted X chromosome expression. In this study, we used an independent cross to help disentangle the effects of regulatory disruption at different developmental stages of spermatogenesis. We used strains of mice that produce subfertile hybrid males in both cross directions, but only offspring from *musculus* females and *domesticus* males have a *Sly* deficit. We found that both reciprocal hybrids showed disrupted MSCI, consistent with *Prdm9*-associated sterility. However, only the hybrids that had the greater disruption of MSCI and are *Sly*-deficient showed disrupted postmeiotic X chromosome expression, suggesting that postmeiotic disruption is genotype-specific. Collectively, these results further underscore the considerable genotypic and phenotypic (regulatory and reproductive) variably underlying F1 hybrid sterility between these closely-related mouse lineages.

174

175 ## MATERIALS & METHODS

176 ### Crosses and reproductive phenotypes

177 We used four inbred strains of wild-derived mice from two subspecies of *domesticus* (WSB/EiJ
178 and LEWES/EiJ) and *musculus* (PWK/PhJ and CZECHII/EiJ). First, we generated intraspecific
179 F1s between strains of *domesticus* (WSB females × LEWES males) and *musculus* (CZECHII
180 females × PWK males). These mice served as parental controls for each species, but without
181 the negative effects of inbreeding on male fertility. Second, we generated intersubspecific F1
182 hybrids in reciprocal crosses between one strain of each subspecies (CZECHII females x WSB
183 males and WSB females x CZECHII males, *hereafter*: ♀ mus^{CZII} × ♂ dom^{WSB} and ♀ dom^{WSB} ×
184 ♂ mus^{CZII}; throughout the manuscript we will indicate all crosses as female parent × male
185 parent). We chose crosses involving CZECHII mice because F1 hybrid males from these
186 crosses are subfertile in both directions of the cross (Good *et al.* 2008b; Larson *et al.* 2018b).
187 This provided a direct contrast to other studies using strains that produce subfertile F1 hybrid
188 males in only one cross direction, (*i.e.* PWK females x LEWES males, Good *et al.* 2010;
189 Campbell *et al.* 2013; Mack *et al.* 2016; Larson *et al.* 2017), which allowed us to begin to isolate
190 the effects of disrupted MSCI and imbalanced copy numbers of *Slx* and *Sly* on regulatory
191 phenotypes. Experimental mice used in this study were obtained from breeding colonies
192 established from mice purchased from The Jackson Laboratory (Bar Harbor, ME) in 2010 and
193 were maintained at the University of Montana Department of Laboratory Animal Resources
194 (IACUC protocol 002-13). One *domesticus* mouse had a sire from replacement stock of
195 LEWES/EiJ ordered in 2013. The stock origin for each mouse is indicated in **Table S1**.
196 We weaned experimental mice at ~21 days after birth and housed them in same sex
197 sibling groups until males were individually isolated at 45 days. We euthanized males between

61 and 89 days old using CO_2 followed by cervical dislocation. Immediately after euthanasia we quantified male reproductive traits following previously described protocols (Good *et al.* 2008b, 2008a). We weighed paired testes and seminal vesicles relative to body weight and isolated sperm by dicing the caudal epididymides in 1 mL of Dulbecco's PBS (Sigma) followed by a 10 min incubation at 37°C. We estimated the proportion of motile sperm and total sperm numbers using 5 μL sperm suspensions (regular and heat-shocked, respectively) viewed in a Makler counting chamber on a light microscope over a fixed area and observation time. We fixed and stained 25 μL sperm suspensions and later counted 100 intact sperm to visually classify morphology. All samples were counted by a single individual (E.L.L.) while blind to genotype. We classified sperm as (1) normal with a long apical hook, (2) slightly abnormal with a shortened hook, (3) abnormal with a short hook and rounded shape, and (4) severely abnormal with an amorphous shape. We summarized sperm morphology using a weighted index that ranged from high (3) to low (0) following Oka *et al.* (2004) and Good *et al.* (2008a).

RNA sequencing of spermatogenesis stages

Testes are composed of at least eleven major cell types, with cell-specific patterns of gene expression (Margolin *et al.* 2014; Green *et al.* 2018). Whole testes expression patterns can be confounded by differences in cell composition between species, or between sterile and fertile hybrids (Good *et al.* 2010; Hunnicutt *et al.* 2021). To overcome these challenges, we used fluorescence activated cell sorting (FACS) to isolate highly enriched cell populations for three developmental stages of spermatogenesis: early prophase of meiosis I prior to MSCI (leptotene/zygotene cells), meiosis I after MSCI (diplotene cells) and postmeiotic development prior to spermiogenesis (round spermatids). Our complete FACS protocol, modified from Getun *et al.* (2011), is available on Github (https://github.com/goodest-goodlab/good-

protocols/tree/main/protocols/FACS). We decapsulated the testes and disassociated them in a mixture of 1 mg/mL collagenase (Worthington Biochemical), GBSS (Sigma) and 1 mg/mL trypsin (Worthington Biochemical). We inactivated the trypsin with 0.16 mg/mL fetal calf serum (Sigma) and stained the cells with 0.36 mg/mL of Hoechst 33343 (Invitrogen) and 0.002 mg/mL propidium iodide. At each step, we incubated solutions in a mini shaker at 120 rpm at 33°C for 15 min and added 0.004 mg/mL DNase to eliminate clumps. We filtered disassociated cells twice using a 40 μm strainer and sorted cells on a FACSAria IIu cell sorter (BD Biosciences) at the UM Center for Environmental Health Sciences Fluorescence Cytometry Core. FACS isolates cells based on size, granularity, and fluorescence (traits that change across different stages of spermatogenesis). We collected enriched cell populations in 15 μL beta mercaptoethanol (Sigma) per mL of RLT lysis buffer (Qiagen) and extracted RNA from each cell type using a Qiagen RNeasy kit. We quantified our samples on a Bioanalzyer 2000 (Agilent) and prepared samples with RNA integrity (RIN) above 8 for sequencing using an Illumina Truseq Sample Prep Kit v2 in a design that avoided batch effects between cell populations and genotypes. We extracted RNA from a total of 21 mice, using the highest quality enriched cell populations to generate RNAseq libraries for three individuals per cell type, three cell types and four crosses (*domesticus*, *musculus* and their reciprocal F1 hybrids, $n = 36$ RNAseq libraries).

We sequenced each library on an Illumina HiSeq 2500 (SE, 100 bp) at the University of Oregon Genomics and Cell Characterization Core Facility and on an Illumina HiSeq 2000 (PE, 100 bp) and a NextSeq 500 (SE, 100 bp) at the University of Southern California Epigenome Center. While all of the RNAseq libraries in this study were prepared simultaneously, we previously published a subset of these data, the *domesticus* and *musculus* parent samples, as part of a study on the rate of molecular evolution in spermatogenesis (Larson *et al.* 2016). Here

we focus on comparisons between reciprocal F1 hybrids (unpublished data) and their parents, to disentangle the effects of different developmental stages on regulatory disruption in hybrids.

Read mapping and differential expression analyses

We trimmed reads using TRIMMOMATIC v0.32 (Bolger *et al.* 2014) and mapped reads using TOPHAT v2.0.10 (Kim *et al.* 2013) to strain-specific pseudo-references for *domesticus* (WSB/EiJ) and *musculus* (PWK/PhJ) (Huang *et al.* 2014). These pseudo-references incorporate all known SNPs, indels and structural variants for these strains relative to the Genome Reference Consortium mouse build 38 (GRCm38), thereby minimizing mapping bias to the mouse reference genome, which is predominately *domesticus* (Yang *et al.* 2011). We used LAPELS v1.0.5 to translate our reads back into the GRCm38 coordinates and SUSPENDERS v0.2.4 to merge our alignments (Huang *et al.* 2014). We counted the number of reads that mapped to protein-coding genes (Ensembl release 78) using FEATURECOUNTS v1.4.4 (Liao *et al.* 2014). We counted reads that were 1) uniquely mapped to a single protein-coding gene and 2) mapped to multiple protein-coding genes. These two approaches were qualitatively the same, but by including multi-mapped reads we could account for the expression of multicopy gene families that are enriched on the mouse X chromosome, and in all cases we report these results.

We analyzed gene expression using Bioconductor v3.0 package edgeR v3.30.3 (Robinson *et al.* 2010) in R v4.0.1 (R Core Team 2020). We normalized our data using the scaling factor method and restricted our analysis to genes with a minimum expression of FPKM > 1 in at least three samples. For all analyses, we tested alternative normalization methods (*e.g.,* weighted trimmed mean of M-values) and found qualitatively similar results. We fit our data with a negative binomial generalized linear model with Cox-Reid tagwise dispersion estimates (McCarthy *et al.* 2012). Our model included cross and cell type as a single factor and

our design matrix contrasted different crosses for each cell type. To evaluate differential expression, we used likelihood ratio tests, dropping one coefficient from the design matrix and comparing that to the full model. For each contrast, we restricted our differentially expressed (DE) genes to genes that are expressed in the focal cell type (FPKM > 1 in 3/6 samples) and in all cases used a p-value adjusted for a false discovery rates (FDR) of 5% (Benjamini and Hochberg 1995). For all our RNAseq analysis, we focused on contrasts between each hybrid and their parental X chromosome, to account for potential mapping biases on the hemizygous X (♀ *mus*^{CZII} × ♂ *dom*^{WSB} vs. *musculus*; ♀ *dom*^{WSB} × ♂ *mus*^{CZII} vs. *domesticus*) and contrasts between the two F1 hybrids (♀ *mus*^{CZII} × ♂ *dom*^{WSB} vs. ♀ *dom*^{WSB} × ♂ *mus*^{CZII}).

We used a sliding gene window to test for local enrichment of autosomal genes that were overexpressed in round spermatids of ♀ *mus*^{CZII} × ♂ *dom*^{WSB} hybrids compared to ♀ *dom*^{WSB} × ♂ *mus*^{CZI} hybrids. We counted the proportion of genes that were up (+logFC) or down (-logFC) regulated within a given window and identified windows that fell outside of the 99th quantile modeled with a Poisson distribution. We tested a range of window sizes (50-400 genes/window) and found qualitatively similar results, so we used 250 genes/window. This method has been previously used to identify overexpression of an ampliconic autosomal gene family, *α-takusan* in sterile *musculus* x *domestics* hybrids (Larson et al. 2017).

Sequencing of *Prdm9* alleles

We characterized the *Prdm9* Exon12 allele for each strain used in our study. For each strain, we extracted DNA from liver tissue of a single mouse using a Nucleospin Tissue Kit (Macherey-Nagel) and quantified the DNA with a QuantiFluor dsDNA System (Promega) on a Synergy HTX Multi-Mode Microplate Reader (Agilent). We amplified *Prdm9* Exon12 using the primers Exon12-L1 and Exon12-R (Mukaj *et al.* 2020), GoTaq Polymerase (Promega) and the following

294 protocol: an initial denaturation at 95°C for 2 min, followed by 41 cycles of 95°C for 30 s, 56°C
295 for 30 s, and 72°C for 1 min, with a final extension step of 72°C for 5 min. We purified and
296 sequenced amplicons at Genewiz (New Jersey, USA), using their hairpin sequencing. We
297 manually cleaned and translated sequences in Geneious 9.1.8 (Biomatters) and aligned
298 sequences using MAFFT v7.453 (Katoh and Standley 2013). We identified C-terminal zinc
299 finger domains by searching sequences with hmmsearch for the Zf-C2H2 HMM profile
300 (PF00096.27) from the Pfam database (HMMER v3.3.2; Mistry *et al.* 2021). We excluded the
301 first nonvariant zinc finger domain then compared the -1, 3, and 6 positions within each domain
302 (as in Oliver *et al.* 2009) to previously published *musculus* and *domesticus* alleles (Mukaj *et al.*
303 2020).
304
305 **Gene Copy Number Estimates**
306 To estimate *Slx* and *Sly* gene copy numbers, we generated whole genome sequence data from
307 a single mouse of each strain used in our study (*domesticus* WSB/EiJ, LEWES/EiJ and
308 *musculus* PWK/PhJ and CZECHII/EiJ). For each sample, we prepared and sequenced libraries
309 twice to increase unique read coverage. We extracted DNA from liver tissue using a Qiagen
310 DNeasy kit and sent samples to Novogene for library preparation and sequencing on an Illumina
311 NovaSeq 6000 (PE, 150bp). We trimmed reads with TRIMMOMATIC v0.39 (Bolger *et al.* 2014),
312 mapped our reads to the GRCm38 using BWA-MEM v0.7.17 (Li and Durbin 2009), and fixed
313 mates and marked duplicates with Picard v2.18.29 (Broad Institute 2019). We merged the data
314 from each sequencing effort resulting in 10-15X average genome-wide coverage.
315 To identify paralogs of ampliconic gene families, we extracted *Slx*, *Slxl1*, and *Sly* gene
316 sequences from the mouse reference GRCm38 using Ensembl release 102 (Yates *et al.* 2019).
317 We performed Ensembl BLAT searches with these sequences against the GRCm38 mouse
318 reference, allowing up to 1000 hits. We then extracted all BLAT hits with greater than or equal to

97% sequence identity and an e-value of 0.0 and considered these filtered BLAT hits to be gene family paralogs for downstream copy number estimation.

We estimated copy number using two methods based on relative coverage. First, we followed a similar approach as Morgan and Pardo-Manuel de Villena (2017) and used Mosdepth (Pedersen and Quinlan 2018) to estimate coverage in paralog regions and the average coverage across the whole genome. We estimated copy number by summing coverage across paralog regions and dividing this sum by half the genome-wide average coverage. We halved the average coverage because most of the mouse genome is diploid, while the sex chromosomes in males are haploid. We also used the approach implemented in AmpliCoNE (Vegesna *et al.* 2019), which estimates copy number from relative coverage using only regions that are considered informative based on repeat masking and mappability, while also controlling for GC content. AmpliCoNE was developed for estimating gene copy numbers on the human Y chromosome, so we made some modifications to account for the less complete assembly and annotation of the mouse sex chromosomes. Specifically, instead of relying on informative sites to differentiate copy numbers, we extracted all kmers of length 101bp from the *Slx*, *Slxl1*, and *Sly* gene sequences and mapped these back to the mouse reference genome using Bowtie2, allowing up to 500 multiple mapping hits. For each gene, we identified the most frequent number of times (*m*) kmers mapped to the mouse genome and kept only kmers that mapped *m* times. We identified all locations where these kmers mapped with 2 or fewer mismatches and used these kmer start locations as the “informative sites” metric for AmpliCoNE.

Data Availability

The data reported in this paper are available through the National Center for Biotechnology Information Sequence Read Archive under accession numbers PRJNA296926 (*domesticus* and *musculus* RNAseq data), PRJNA352861 (F1 hybrid RNAseq data), PRJNA732719 (lab strain

whole genome sequence data). *Prdm9* sequences were deposited in Genbank under accession numbers MZ733983-MZ733986. Male reproductive phenotype data are available in **Table S1**.

RESULTS

Hybrid males from both cross directions were subfertile

We found F1 hybrid males from crosses between *domesticus* (WSB) and *musculus* (CZECHII) were subfertile in both cross directions, but that ♀ mus^{CZII} × ♂ dom^{WSB} hybrids had more severe abnormal sperm morphology. Overall, ♀ dom^{WSB} × ♂ mus^{CZII} hybrids had lower fertility than both *domesticus* and *musculus*, with significantly smaller testes, lower sperm counts, and more abnormal sperm morphology, while ♀ mus^{CZII} × ♂ dom^{WSB} hybrids had smaller testes and lower sperm counts, but after correcting for multiple tests these values were only significant in comparisons with *domesticus* (**Table 1**). The ♀ mus^{CZII} × ♂ dom^{WSB} hybrids did have the most severely abnormal sperm morphology consistent with previous studies (Good *et al.* 2008b; Larson *et al.* 2018b). There were no significant differences in the relative seminal vesicle weight or the proportion of motile sperm across any comparisons.

Table 1. Reproductive phenotypes of male mice used in this study. The table summarizes the sample sizes for each cross (N) and the median (± standard error) trait value for five reproductive phenotypes. Arrows indicate whether the hybrids had significantly lower reproductive values relative to *domesticus* (closed arrows) or *musculus* (open arrows). Values in bold indicate traits that were significantly different between the two F1 hybrids. Testes and seminal vesicle weights are reported relative to body size. The sperm morphology index ranged from 3 (high quality sperm) to 0 (severally abnormal sperm). Significance was estimated using a Wilcoxon test with p-values FDR corrected for multiple comparisons.

Cross	N	Relative testis weight (mg/g)	Relative seminal vesicle weight (mg/g)	Proportion motile sperm	Sperm count ($1x10^6$)	Sperm head morphology index
domesticus	6	11.30 ± 0.34	5.18 ± 0.29	0.82 ± 0.04	14.8 ± 1.80	2.99 ± 0.01
musculus	5	9.53 ± 0.63	5.58 ± 1.30	0.87 ± 0.06	17.8 ± 2.50	3.00 ± 0.03
♀ *dom*^{WSB} × ♂ *mus*^{CZII}	6	▼▽6.28 ± 0.28	5.68 ± 0.54	0.83 ± 0.06	▼▽4.2 ± 0.72	▼▽**1.29 ± 0.07**
♀ *mus*^{CZII} × ♂ *dom*^{WSB}	4	▼6.46 ± 0.35	5.44 ± 0.27	0.65 ± 0.12	▼5.8 ± 2.70	▼▽**0.66 ± 0.12**

Cell-specific gene expression

For each cross, we generated between 14.7 and 26.8 million mapped fragments (paired or unpaired reads) per cell type (738 million total, mean = 20.5 million). After filtering we retained 14,209 expressed protein-coding genes. Gene expression profiles clustered by cell type (**Fig S1A**) and within each cell type, samples clustered by parental species with F1 hybrids intermediate to the two parents (**Fig S1B-D**). Overall, the strong clustering by cell type and cross, and the overall low variation among our samples (biological coefficient of variation = 0.1748), indicates our FACS approach generated high quality cell-specific data.

Disrupted meiotic X inactivation in both subfertile hybrids

We found disrupted meiotic X chromosome inactivation (diplotene cells) in both subfertile hybrids, but the disruption was more severe in ♀ *mus*^{CZII} × ♂ *dom*^{WSB} hybrids. Consistent with previous results (Larson *et al.* 2016, 2017), fertile *domesticus* and *musculus* males had very few X-linked genes expressed in diplotene cells. In contrast, both F1 hybrids had elevated expression of X-linked genes in diplotene cells (**Fig S2**), consistent with disrupted MSCI. In comparisons between F1 hybrids and their parents with the same X chromosome (♀ *mus*^{CZII} × ♂ *dom*^{WSB} vs. *musculus*; ♀ *dom*^{WSB} × ♂ *mus*^{CZII} vs. *domesticus*), F1 hybrids expressed more X-linked genes and every differentially expressed (DE) gene was overexpressed in hybrids. In

387 contrast, there was no obvious asymmetry in expression on the autosomes (**Figs 1A, B**). When
388 we compared the two hybrids, ♀ *mus*^{CZII} × ♂ *dom*^{WSB} had higher X-linked expression and DE
389 genes between the hybrids were largely overexpressed in ♀ *mus*^{CZII} × ♂ *dom*^{WSB} hybrids (**Fig**
390 **1C**), suggesting that disrupted MSCI was more severe in ♀ *mus*^{CZII} × ♂ *dom*^{WSB} hybrids.
391
392 **Reciprocal hybrids have identical *Prdm9* genotypes**
393 We characterized all four strains for allelic variation within Exon12 of *Prdm9* and confirmed that
394 both *musculus* strains (PWK and CZECHII) shared the same *msc1* 'sterile' allele and both
395 *domesticus* strains (WSB and LEWES) shared the same 'sterile' *dom3 Prdm9* allele (Forejt *et*
396 *al.* 2021). Therefore, both ♀ *mus*^{CZII} × ♂ *dom*^{WSB} and ♀ *dom*^{WSB} × ♂ *mus*^{CZII} hybrids have the
397 same *Prdm9* genotype at Exon12 (*msc1*/*dom3*).

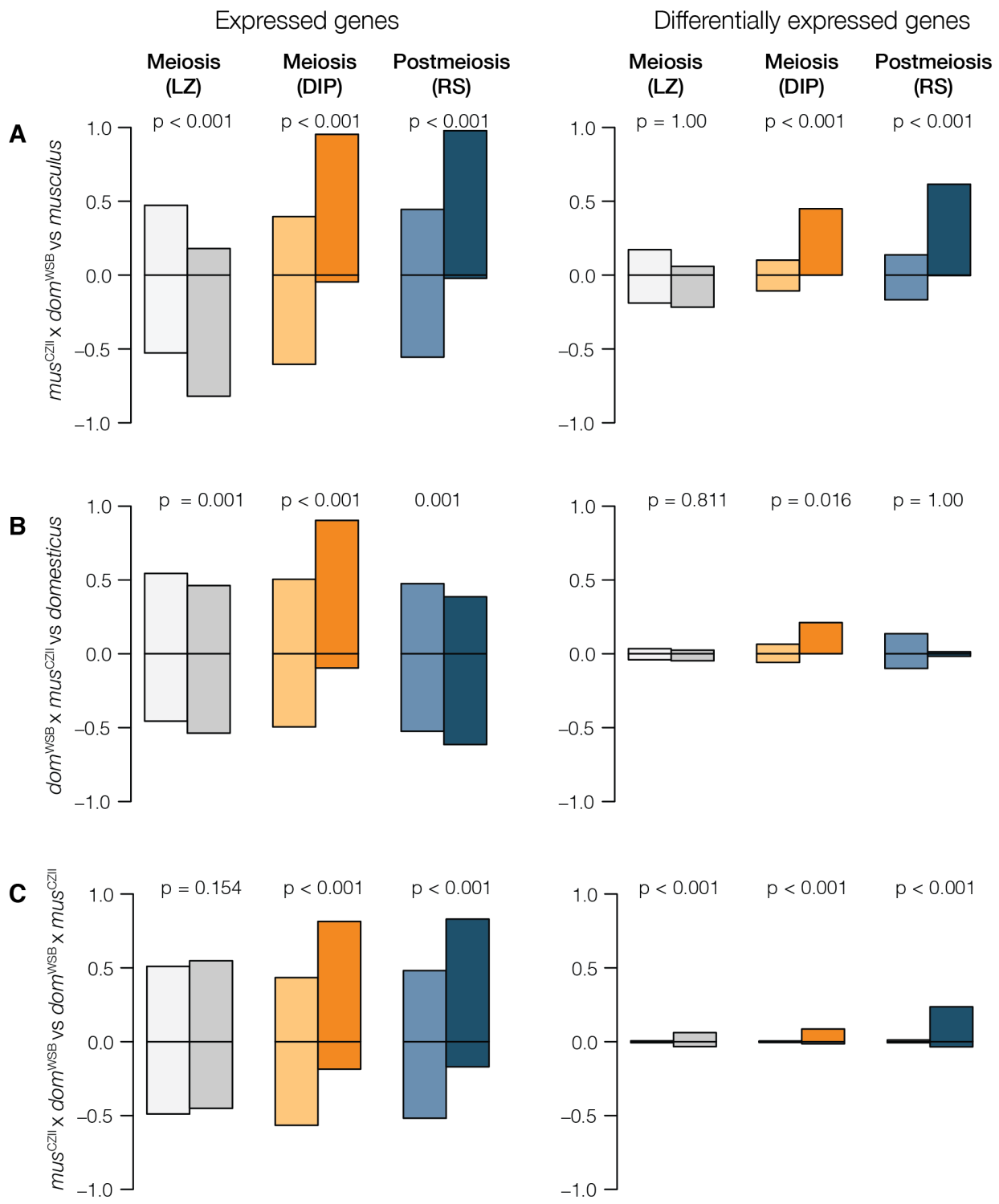

Fig 1. Gene expression comparisons among hybrids and parents for autosomes (light colors) and the X chromosome (dark colors). There are three contrasts: **A)** ♀ *mus*^{CZII} × ♂ *dom*^{WSB}

401 hybrids compared to *musculus* , **B)** ♀ *dom*^{WSB} × ♂ *mus*^{CZII} hybrids compared to *domesticus*, **C)**
402 ♀ *mus*^{CZII} × ♂ *dom*^{WSB} hybrids compared to ♀ *dom*^{WSB} × ♂ *mus*^{CZII} hybrids. The first column
403 shows the proportion of genes with higher or lower expression in a given contrast out of the total
404 genes expressed in each cell type. The second column shows the proportion of those genes
405 that are DE. Significant p-values indicate contrasts where there was a significant difference in
406 the proportion of over or underexpressed genes on the X chromosome compared to the
407 autosomes (Pearson's chi square test with FDR corrected p-values, Benjamini and Hochberg
408 1995). LZ = leptotene/zygotene cells (meiosis before MSCI), DIP = diplotene cells (meiosis after
409 MSCI), RS = round spermatids (postmeiosis).
410

411 **Imbalanced *Sly* and *Slx/Slxl1* copy numbers in reciprocal hybrids**

412 We estimated gene copy number for postmeiotic amplicon families in our mouse strains using
413 two methods and found that *musculus* had higher copy number for *Sly*, *Slx*, and *Slxl1* (**Table 2**).
414 Our copy number estimates for *Sly* and *Slx* differed from what has been estimated using qPCR
415 (Ellis *et al.* 2011) - we found higher copy numbers of *Sly* and lower copy numbers of *Slx*. Our
416 estimates were closer to those from other studies that have used a computational approach to
417 estimate copy number (Morgan and Pardo-Manuel de Villena 2017) and were similar to
418 estimates for the *domesticus* Y chromosome assembly (Soh *et al.* 2014). Both our results and
419 these other studies consistently found higher copy numbers in *musculus*, indicating there is an
420 imbalance in *Sly* and *Slx/Slxl1* copy numbers of F1 hybrids relative to parental strains.

421
422
423

Table 2: Copy number estimates for the *Sly* and *Slx/Slxl1* gene families for the wild-derived mouse strains used in this study.

		Mosdepth			AmpliCoNE		
		Sly	***Slx***	***Slxl1***	***Sly***	***Slx***	***Slxl1***
musculus	CZECHII	206	51	34	217	62	38
	PWK	192	48	34	213	50	38
domesticus	LEWES	152	16	22	134	15	20
	WSB	155	13	29	127	13	25

Postmeiotic disruption in *Sly*-deficient hybrids

The X chromosome was overexpressed in postmeiotic round spermatids of ♀ *mus*^{CZII} × ♂ *dom*^{WSB} hybrids (*Sly*-deficient), but not in ♀ *dom*^{WSB} × ♂ *mus*^{CZII} hybrids (*Slx*-deficient). Nearly all of the X-linked postmeiotic genes in ♀ *mus*^{CZII} × ♂ *dom*^{WSB} hybrids were overexpressed relative to *musculus* and more than half of these were DE (**Fig 1A**). In contrast, ♀ *dom*^{WSB} × ♂ *mus*^{CZII} hybrids had genes that were both over- and under-expressed relative to *domesticus* and DE genes tended to be expressed at lower levels (although this pattern wasn't significant) (**Fig 1B**). There were no clear asymmetries on the autosomes for either hybrid relative to their parent. Given that both hybrids showed some degree of disrupted expression in meiotic cells, this suggests postmeiotic disruption is not a simple downstream consequence of earlier MSCI disruption, but is either an independent mechanism for postmeiotic disruption in *Sly*-deficient hybrids or there is a threshold of disrupted MSCI required to lead to downstream disruption.

SLX/SLXL1 and SLY compete for interaction with SSTY1 at promotors to regulate a suite of postmeiotic multicopy genes, including autosomal gene families *α-takusan* and *Speer*

(Moretti *et al.* 2017, 2020). To test if we could detect misexpression of these autosomal gene families in our *Sly*-deficient hybrids, we used a sliding gene-window analysis (250 genes/window) to identify genomic regions with clusters of over or under-expressed genes between our reciprocal F1 hybrids. We found two small gene windows on chromosomes 5 and 8 that exceeded our threshold for overexpressed gene-windows (99th quantile modeled with a Poisson distribution) (**Fig S3**), but these regions did not overlap with any known multicopy gene families. We did not detect any large gene-windows that were consistently overexpressed in *Sly*-deficient hybrids as we did in crosses between *mus*^{PWK} x *dom*^{LEW} (Larson *et al.* 2017).

Comparison of patterns of disrupted X expression across different hybrid genotypes

Finally, we used previously published data from Larson et al. 2017 to compare overlap in X-linked DE genes between reciprocal subfertile hybrids in this study (♀ *mus*^{CZII} × ♂ *dom*^{WSB}, ♀ *dom*^{WSB} × ♂ *mus*^{CZII}) with other subfertile hybrids (♀ *mus*^{PWK} × ♂ *dom*^{LEW}). We found the greatest number of X-linked DE genes in postmeiotic round spermatids of ♀ *mus*^{CZII} × ♂ *dom*^{WSB} hybrids, and many of these same genes were also DE in ♀ *mus*^{PWK} x ♂ *dom*^{LEW} hybrids (**Fig 2**). The second highest number of X-linked DE genes were in meiotic cells (diplotene) of *mus*^{PWK} x *dom*^{LEW} hybrids, and a subset of these genes were also DE in ♀ *mus*^{CZII} × ♂ *dom*^{WSB} hybrids. There were approximately half as many DE meiotic genes in ♀ *dom*^{WSB} × ♂ *mus*^{CZII} hybrids, but nearly all of these were also misexpressed in the meiotic cells of the other two *mus* x *dom* hybrids. There were very few X-linked DE genes in the postmeiotic cells of ♀ *dom*^{WSB} × ♂ *mus*^{CZII} hybrids, though these genes did tend to overlap with DE postmeiotic genes in the other two subfertile hybrids.

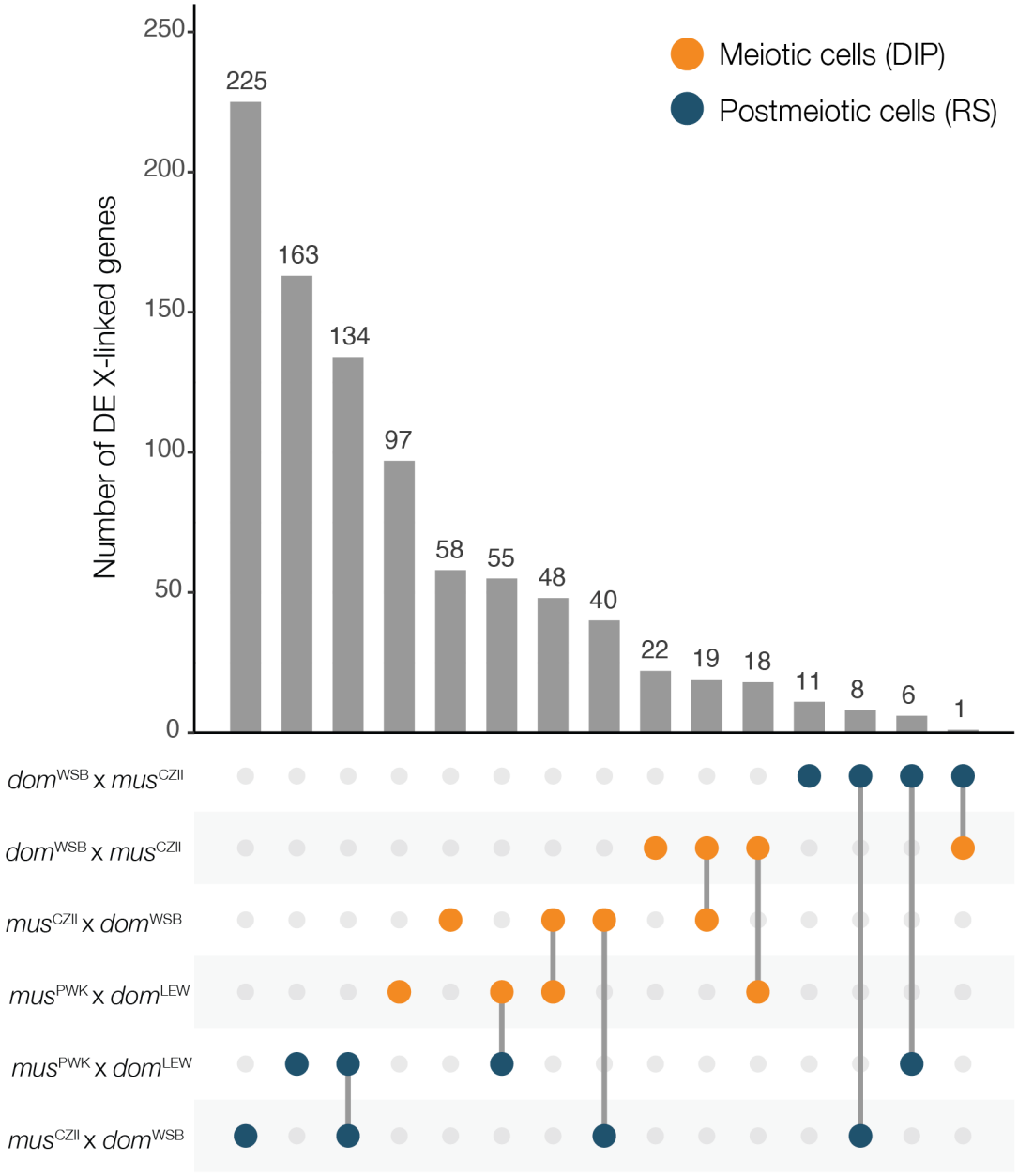

464

465 **Fig 2. Number of X-linked DE genes across multiple subfertile hybrids.** The dots indicate a
466 contrast between a subfertile hybrid and its respective parental X chromosome and the barplot
467 indicates the number of X-linked DE genes in that contrast. When there are two contrasts listed
468 and a line connecting them it indicates the number of DE X-linked genes that are overlapping
469 between the two contrasts. DIP = diplotene cells (orange), RS = round spermatids (blue).

470

DISCUSSION

Disrupted meiotic X inactivation in reciprocal F1 hybrids

Disruption of spermatogenesis during early meiosis has been linked to PRDM9, a protein that directs the location of meiotic recombination (Mihola *et al.* 2009). Divergence at PRDM9 DNA-binding sites can lead to incomplete meiotic synapsis of homologous chromosomes (Bhattacharyya *et al.* 2013; Davies *et al.* 2016; Gregorova *et al.* 2018), and associated disruption of MSCI (Good *et al.* 2010; Bhattacharyya *et al.* 2013; Campbell *et al.* 2013; Turner *et al.* 2014; Mack *et al.* 2016; Larson *et al.* 2017). We found disrupted MSCI in reciprocal subfertile hybrids, consistent with *Prdm9*-associated sterility in both F1 hybrids. Overall, the disruption was greater in ♀ *mus*^{CZII} × ♂ *dom*^{WSB} hybrids, but meiotic arrest was not complete in either cross, suggesting variation in the mechanisms that contribute to *Prdm9*-associated sterility.

PRDM9 defines where meiotic recombination will occur by adding histone marks that guide SPO11 protein to induce double-strand breaks, which are repaired as either crossovers or non-crossovers (Baudat *et al.* 2010; Myers *et al.* 2010; Parvanov *et al.* 2010). The C-terminal zinc finger domain of PRDM9 determines its binding affinity to a particular site, but *Prdm9* binding sites evolve very rapidly due to biased gene conversion. If one homolog has a mutation at a PRDM9 binding site, then PRDM9 will bind preferentially to the other homolog with the ancestral binding site, causing double strand break formation in only one chromosome. This break will be repaired using the mutated strand as a template, thus mutations at PRDM9 binding sites are rapidly incorporated into both homologs, leading to the erosion of PRDM9 binding sites over time (Myers *et al.* 2010; Baker *et al.* 2015). The same mechanism is what leads to autosomal asynapsis in hybrids (Smagulova *et al.* 2016; Davies *et al.* 2016; Gregorova *et al.* 2018). When hybrids are heterozygous at *Prdm9* and at PRDM9 binding-sites throughout the genome, PRDM9 binds preferentially to its ancestral binding sites, leading to asymmetric

formation of double strand breaks, and the failure of autosomes to properly synapse. Asynapsed autosomes interfere with normal MSCI leading to the overexpression of the X chromosome, although the exact mechanism is still unknown (Forejt *et al.* 2021). Consistent with this model, we found reciprocal F1 hybrids both had disrupted MSCI and we found the same X-linked genes had disrupted meiotic X expression in both crosses, although there were slightly more disrupted genes in *mus*^{PWK} x *dom*^{LEW} hybrids (**Fig 2**). This suggests asymmetric PRDM9 binding occurs in both cross directions.

Prdm9-associated sterility is also influenced by an interaction with the *Hstx2* locus, a ~2.7 Mb region in the middle of the X chromosome (Storchová *et al.* 2004; Bhattacharyya *et al.* 2014; Lustyk *et al.* 2019). Complete meiotic arrest typically only occurs in F1 mice with a *musculus Hstx2* allele (*i.e., musculus* X chromosome), while F1 mice with a *domesticus* X chromosome may vary from subfertile to nearly fully fertile (Dzur-Gejdosova *et al.* 2012; Flachs *et al.* 2012; Mukaj *et al.* 2020). The *Hstx2* locus harbors a gene, *Meir1* that controls recombination rates, and is a strong candidate for directly modulating PRDM9 binding (Dumont and Payseur 2011; Balcova *et al.* 2016). This model predicts that sterility and disrupted gene expression will be the most severe in F1 hybrids with a *musculus* X chromosome. When we have examined expression in enriched cell populations, hybrids from *musculus* x *domesticus* crosses were subfertile and had disrupted MSCI (♀ *mus*^{CZII} × ♂ *dom*^{WSB}, this study; *mus*^{PWK} x *dom*^{LEW}, Larson *et al.* 2017), while some reciprocal hybrids were fertile with normal MSCI (*dom*^{LEW} x *mus*^{PWK}, Larson *et al.* 2017). Indeed, we found that disrupted MSCI was much less severe in ♀ *dom*^{WSB} x ♂ *mus*^{CZII} hybrids (**Fig 2**), consistent with the idea that the *musculus* X chromosome is required for more severe meiotic disruption.

The severity of sterility in *musculus* x *domesticus* crosses appears to depend on allelic variation at *Prdm9* (Chromosome 17) and/or *Hstx2* (X chromosome). The PRDM9 C-terminal

519 zinc finger domain is composed of repeats that are polymorphic within each subspecies (Buard
520 *et al.* 2014; Kono *et al.* 2014; Vara *et al.* 2019) and 'fertile' and 'sterile' alleles have been
521 described in both *musculus* and *domesticus* (Flachs *et al.* 2012; Mukaj *et al.* 2020). The strains
522 we used in this study appear to have identical *Prdm9* alleles to those that have been described
523 as 'sterile' in other studies (Mukaj *et al.* 2020; see also Forejt *et al.* 2021). Thus, despite both
524 reciprocal hybrids having identical *Prdm9* genotypes (*msc1*/*dom3*), ♀ *mus*^{CZII} × ♂ *dom*^{WSB}
525 produce some sperm with normal morphology (Table 1), suggesting that other loci must
526 modulate *Prdm9*-associated sterility in this cross. In *musculus* PWK x *domesticus* B6 hybrids
527 with two 'sterile' Prdm9 alleles, partial fertility appears to be associated with allelic variation on
528 the X chromosome (Flachs *et al.* 2014), possibly at the *Hstx2* locus. Allelic variation on the X
529 chromosome may also explain why complete meiotic arrest was not found in crosses with wild-
530 derived strains in this study (♀ *mus*^{CZII} × ♂ *dom*^{WSB}), by Larson et al. (2017; ♀ *mus*^{PWK} x
531 ♂ *dom*^{LEW}), and in some other *musculus* x *domesticus* crosses with two 'sterile' *Prdm9* alleles
532 (Mukaj *et al.* 2020).

533 Allelic variation at *Prdm9* could also explain the subfertility of ♀ *dom*^{WSB} × ♂ *mus*^{CZII}
534 hybrids, in the absence of the *musculus* X chromosome. F1 *domesticus* x *musculus* hybrids can
535 be subfertile when both *Prdm9* alleles are 'sterile' (Flachs *et al.* 2012). The combination of two
536 sterile *Prdm9* alleles and heterozygous PRDM9 binding sites throughout the genome may be
537 sufficient to disrupt MSCI in ♀ *dom*^{WSB} × ♂ *mus*^{CZII} hybrids. However, it is unclear why MSCI
538 would be disrupted in ♀ *dom*^{WSB} × ♂ *mus*^{CZII} hybrids, but not ♀ *dom*^{LEW} × ♂ *mus*^{PWK} hybrids,
539 which also have two sterile *Prdm9* alleles. It is also unknown to what extent *Prdm9* contributes
540 to the sterility phenotypes in ♀ *dom*^{WSB} × ♂ *mus*^{CZII} hybrids, given that other autosomal sterility
541 factors have been mapped in ♀ *dom*^{WSB} × ♂ *mus*^{CZII} hybrids to chromosomes 2, 8 and 9 (Larson
542 *et al.* 2018b).

In addition to allelic variation, the outcome of *Prdm9*-associated sterility is likely to be variable across cells within an individual. *Prdm9*-induced autosomal asynapsis is a threshold response. If a sufficiently large number of autosomes fail to pair (asynapsis rates > 60%) it leads to full meiotic arrest, while lower rates of asynapsis may lead to intermediate levels of meiotic disruption (Bhattacharyya *et al.* 2013; Mukaj *et al.* 2020). While MSCI is disrupted in ♀ *mus*^{CZII} × ♂ *dom*^{WSB} hybrids, the X chromosome still had lower expression in meiosis compared to other cell types (**Fig S2**) and a similar pattern was found for disrupted MSCI in ♀ *mus*^{PWK} x ♂ *dom*^{LEW} hybrids (Larson *et al.* 2017). This suggests cell-to-cell variation in the occurrence or magnitude of disrupted MSCI which may contribute to the range of sperm morphologies found in these hybrids - from severely impaired to apparently normal (**Table 1**).

Asymmetric disruption of postmeiotic expression suggests genotype-specific hybrid sterility regulatory phenotypes

Postmeiotic disruption of X chromosome expression was observed in ♀ *mus*^{CZII} × ♂ *dom*^{WSB} hybrids but not in reciprocal ♀ *dom*^{WSB} × ♂ *mus*^{CZII} hybrids (**Fig 1A, 1B**). Both F1 hybrids had earlier disruption of MSCI, which suggests that postmeiotic overexpression of the X chromosome is not a simple downstream consequence of disruption at earlier developmental timepoints. It is possible that downstream postmeiotic disruption depends on the magnitude of disrupted MSCI, or the disruption of particular X-linked genes or gene networks. Consistent with this, ♀ *mus*^{CZII} × ♂ *dom*^{WSB} hybrids had a higher proportion of disrupted X-linked genes in meiosis.

Asymmetric postmeiotic disruption is also consistent with antagonistic coevolution of X- and Y-linked multicopy gene families that leads to overexpression only in one cross direction. We found the X chromosome was overexpressed in postmeiotic cells of F1 hybrids that had a

deficit of the Y-linked gene family *Sly* (♀ *mus*^{CZII} × ♂ *dom*^{WSB} hybrids), but not in reciprocal F1 hybrids that had a deficit of the X-linked gene family *Slx/Slxl1* (♀ *dom*^{WSB} × ♂ *mus*^{CZII} hybrids)(**Fig 1A, 1B**). *Sly* and *Slx/Slxl1* play a major role in suppressing or promoting postmeiotic expression of multi-copy sex-linked and interacting autosomal genes (Mueller *et al.* 2008, 2013, Kruger *et al.* 2019, Moretti *et al.* 2020). Imbalanced copy numbers of these genes in F1 hybrids may also disrupt postmeiotic expression networks. This could happen either independently of upstream meiotic disruption, or there may be an interaction among X-linked regulatory networks at different stages of development.

Slx/Slxl1 originated from a single copy autosomal gene (*Sycp3*) that was transposed to the X chromosome (*Slxl1* then *Slx*) and eventually a copy emerged on the Y chromosome (*Sly*) (Kruger *et al.* 2019) . Since their origin, these genes, additional sex-linked ampliconic genes, and associated autosomal ampliconic genes have undergone a massive co-amplification in different mouse lineages leading to divergent copy numbers in *domesticus* and *musculus* (see Table 2; Ellis *et al.* 2011; Turner *et al.* 2014; Soh *et al.* 2014; Morgan and Pardo-Manuel de Villena 2017). *Slx* and *Sly* appear to coevolve in a copy number arms race for interaction with SSTY1 at the promoter of thousands of postmeiotic genes (Moretti *et al.* 2020). Knockdown of *Sly* expression or duplications of *Slx/Slxl1* (i.e., *Sly*-deficient) leads to increased transmission of the X chromosome, abnormal sperm morphology, and upregulation of multicopy genes on the sex chromosomes (Cocquet *et al.* 2009, Kruger *et al.* 2019), as well as upregulation of the autosomal *Speer* (Chr 5) and *α-takusan* (Chr 14) gene families (Moretti *et al.* 2020). Knockdown of *Slx/Slxl1* expression (*i.e. Slx*-deficient) suppresses postmeiotic multicopy gene expression and leads to increased transmission of the Y chromosome and mild sperm abnormalities (Cocquet *et al.* 2010, 2012; Kruger *et al.* 2019). Reciprocal F1 hybrids between *domesticus* (*Sly* 130, *Slx/Slx1* 35, *Sly/Slx* ratio: 3.7) and *musculus* (*Sly* 215, *Slx/Slx1* 100, *Sly/Slx* ratio: 2.15)

591 mirror these knockdown experiments: F1 hybrids from *musculus* × *domesticus* are *Sly*-deficient
592 (130 *Sly,* 100 *Slx*, *Sly/Slx* ratio: 1.3) and F1 hybrids from *domesticus* × *musculus* are *Slx*-
593 deficient (215 *Sly,* 35 *Slx*, *Sly/Slx* ratio: 6.1, **Table 2**).

594 Consistent with a *Sly/Slx* imbalance, we found *Sly*-deficient ♀ mus^{CZII} × ♂ dom^{WSB}
595 hybrids overexpressed the X chromosome in postmeiotic cells (**Fig 1A**). We saw the same
596 overexpression of the X chromosome in an independent contrast of *Sly*-deficient mus^{PWK} ×
597 dom^{LEW} hybrids (Larson *et al.* 2017). The same X-linked genes were overexpressed in both
598 crosses, though there were more upregulated X-linked genes in ♀ mus^{CZII} × ♂ dom^{WSB} hybrids
599 (**Fig 2**). In contrast, we found very few X-linked DE genes in *Slx*-deficient ♀ dom^{WSB} × ♂ mus^{CZII}
600 hybrids, and there was no asymmetry in the expression of DE genes in ♀ dom^{WSB} × ♂ mus^{CZII}
601 hybrids - genes were both up and down regulated relative to the *domesticus* X chromosome
602 (**Fig 1B**). If anything, X-linked postmeiotic genes tended to be underexpressed in ♀ dom^{WSB} ×
603 ♂ mus^{CZII} hybrids relative to the *domesticus* X chromosome, but, unlike in *Slx*-deficient
604 ♀ dom^{LEW} × ♂ mus^{PWK} hybrids (Larson *et al.* 2017), this pattern was not significant. Still, the
605 handful of X-linked postmeiotic genes that were overexpressed in ♀ dom^{WSB} × ♂ mus^{CZII} hybrids
606 were also upregulated in both *musculus* × *domesticus* hybrids (**Fig 2**).

607 In contrast to results from mus^{PWK} × dom^{LEW} hybrids (Larson *et al.* 2017), we did not find
608 co-overexpression of ampliconic autosomal genes families (*Speer* or *α-takusan*) in ♀ mus^{CZII} ×
609 ♂ dom^{WSB} hybrids. The overexpression of these gene families in *Sly*-deficient hybrids was one of
610 the strongest arguments for an independent mechanism of disrupted X expression in mus^{PWK} ×
611 dom^{LEW} hybrids. This lack of agreement makes it difficult to disentangle disrupted regulatory
612 dynamics of *Sly* and *Slx/Slxl1* from possible downstream disruption of PRDM9 in this cross.

613 However, the clear differences in postmeiotic expression between ♀ *mus*^{CZII} × ♂ *dom*^{WSB} hybrids
614 and ♀ *dom*^{WSB} × ♂ *mus*^{CZII} hybrids indicates that postmeiotic disruption is genotype specific.

615 Whether or not postmeiotic sex chromosome overexpression contributes to sterility
616 phenotypes in wild hybrids is still unknown. In knockdown studies, *Sly* and *Slx/Slxl1* have a
617 major impact on sperm morphology (Cocquet *et al.* 2009, 2010, 2012; Kruger *et al.* 2019), but
618 the extent to which these genes might contribute to hybrid sterility phenotypes in wild mice is
619 still unclear (Campbell *et al.* 2013). In knockdown studies, *Sly*-deficient mice have severe sperm
620 deformities (Cocquet *et al.* 2009) and biased X chromosome transmission, while *Slx*-deficient
621 mice tend to have more typical sperm (but see Kruger *et al.* 2019) and biased Y chromosome
622 transmission (Cocquet *et al.* 2010, 2012). The severe sperm deformities in *Sly*-deficient mice
623 appear to particularly affect Y-bearing sperm, decreasing their mobility and providing a direct
624 mechanism for how sperm morphology contributes to sex ratio skews (Rathje *et al.* 2019).
625 However, it is still unclear if the imbalance manifested in mouse hybrids is sufficient to induce a
626 regulatory misexpression phenotype. In F1 hybrids, the imbalanced copy number of *Sly* and
627 *Slx/Slxl1* is certainly less severe in magnitude as total knockdown experiments. If there is a
628 threshold of imbalance required for *Sly* or *Slx/Slxl1* to successfully outcompete the other
629 (Moretti *et al.* 2020), we may not see the same impacts on sperm morphology or sex ratio
630 distortion in wild hybrids. In general, we do find that *Sly*-deficient F1 *musculus* x *domesticus*
631 hybrids have severely abnormal sperm morphology (see Table 1 and Larson *et al.* 2017), while
632 *Slx*-deficient F1 *domesticus* x *musculus* hybrids tend to have more moderate sperm head
633 abnormalities (Larson *et al.* 2017). Similar patterns have been observed in Y introgression lines
634 that mismatch the *musculus* and *domesticus* X and Y chromosomes (Campbell and Nachman
635 2014). In this study, ♀ *dom*^{WSB} × ♂ *mus*^{CZII} hybrids also have severely abnormal sperm head
636 morphology (Table 1), but there are clear autosomal contributions to these abnormalities

637 (Larson *et al.* 2018b). To our knowledge, sex ratio distortion has not been documented in wild-
638 derived crosses, though there is some evidence that it might occur in the mouse hybrid zone
639 (Macholán *et al.* 2008, but see 2019).
640
641 **Conclusions**
642 The elegant *Prdm9* incompatibility model is likely the single most important mechanism
643 of F1 hybrid male sterility in house mice. We find evidence for *Prdm9*-associated disruption of
644 meiosis in subfertile hybrids from reciprocal crosses of two wild-derived strains. We also find
645 evidence that factors outside of *Prdm9* and *Hstx2* contribute to disrupted expression in F1
646 hybrids, providing support for the idea that hybrid sterility is a composite phenotype and likely
647 polygenic (Campbell and Nachman 2014; Larson *et al.* 2017). Other factors such as autosomal
648 incompatibilities and postmeiotic X-Y interactions are likely to be important contributions to
649 overall hybrid sterility. Indeed, the variation we found in the extent and timing of disrupted X
650 expression among different F1 hybrids may reflect interactions among disrupted meiotic and
651 postmeiotic gene networks.
652 The mouse hybrid zone is a relatively recent contact that stretches across central
653 Europe, with a fairly narrow width (Phifer-Rixey and Nachman 2015). Despite the recency of
654 contact and the proximity of parental species, there are few F1 hybrids found in the center of the
655 zone. Instead, the mouse hybrid zone is composed predominantly of advanced generation
656 hybrids and backcrosses (Turner *et al.* 2012; Janoušek *et al.* 2012; Turner and Harr 2014), and
657 hybrid males vary considerably in their fertility (Turner *et al.* 2012). *Prdm9*-associated sterility is
658 strongest in an F1 background with a *musculus* X chromosome and depends on a combination
659 of sterile *Prdm9* alleles (Forejt *et al.* 2021). Stretches of conspecific genomic regions, which are
660 typical for backcrosses and advanced generation hybrids, can rescue meiotic synapsis

(Gregorova *et al.* 2018). As a result, it is very unlikely that *Prdm9* alone can explain the reduced gene flow between *musculus* and *domesticus* in nature.

Studies of differential introgression in the mouse hybrid zone have consistently found the X chromosome to have restricted introgression, as well as a number of different autosomal regions (Tucker *et al.* 1992; Payseur *et al.* 2004; Macholán *et al.* 2007, 2011; Teeter *et al.* 2010; Janoušek *et al.* 2012; Turner and Harr 2014). Restricted introgression can point to regions of the genome that contribute to reproductive barriers. While there is some evidence for premating barriers between *musculus* and *domesticus* (Smadja and Ganem 2002, 2007; Bímová *et al.* 2011; Loire *et al.* 2017), the singular phenotype in all studies of these subspecies is the reduced fertility of hybrid males. Indeed, mapping studies have identified multiple regions of the X chromosome (Oka *et al.* 2004; Good *et al.* 2008a; Dufková *et al.* 2011; Turner *et al.* 2014; Turner and Harr 2014; Morgan *et al.* 2020) and numerous autosomal regions contributing to sterility in F1 hybrids (Larson *et al.* 2018b), F2 crosses and backcrosses (Good *et al.* 2008a; White *et al.* 2011; Turner *et al.* 2014; Schwahn *et al.* 2018; Morgan *et al.* 2020) and wild hybrids (Turner and Harr 2014). There is also evidence that XY mismatch contributing to abnormal sperm morphology (Campbell and Nachman 2014; Martincová *et al.* 2019b, 2019a), and patterns of directional introgression of the *musculus* Y chromosome into *domesticus* backgrounds (Macholán *et al.* 2008, 2019; Ďureje *et al.* 2012), consistent with postmeiotic X and Y chromosome conflict.

Complex hybrid incompatibilities, involving many genes, both autosomal and sex-linked, are a common feature of hybrid male sterility (Coughlan and Matute 2020). The multigenic nature of hybrid male sterility in house mice, and the availability of wild-derived strains makes this an excellent system to identify the genetic basis of hybrid sterility (Forejt *et al.* 2021) and relate these incompatibilities directly to reproductive isolation between natural populations.

AUTHOR CONTRIBUTIONS

JMG conceived of the study and designed the experiments. ELL, EEKK, KEH, DV and SK performed experiments and collected data. ELL, EEKK, and KEH analyzed data. ELL and JMG wrote the manuscript with feedback from all co-authors.

ACKNOWLEDGEMENTS

This work was funded by grants from the Eunice Kennedy Shriver National Institute of Child Health and Human Development of the National Institutes of Health (R01- HD073439, R01-HD094787 to JMG). ELL was supported by the National Science Foundation (DEB 1557059) and EEKK and KEH were both supported by the National Science Foundation Graduate Research Fellowship Program (EEKK: DGE-1313190, and KEH DGE-2034612). We also thank Pamela Shaw and the University of Montana Fluorescence Cytometry Core, supported by the National Institute of General Medicine Sciences of the National Institutes of Health (P30GM103338) for assistance with FACS and the University of Montana Genomics Core, supported by a grant from the M.J. Murdock Charitable Trust. Any opinions, findings, and conclusions or recommendations expressed in this material are those of the author(s) and do not necessarily reflect the views of the National Science Foundation or the National Institutes of Health.

SUPPLEMENTARY DATA

Table S1: Table of individual male reproductive phenotypes (.csv). Table includes each individual mouse ID (*e.g.* CCPP 21.1M stands for dam x sire, litter number, individual number and sex; CC = CZECHII, PP = PWK, WW = WSB, LL = LEWES), cross type, dates the mice were born and phenotype, their age at phenotyping, measures of body size (weight, body length, tail length, right hind foot, left ear length), weights of paired testes and seminiferous vesicles, counts of motile and nonmotile sperm, counts of total sperm, and counts of sperm head morphology categories.

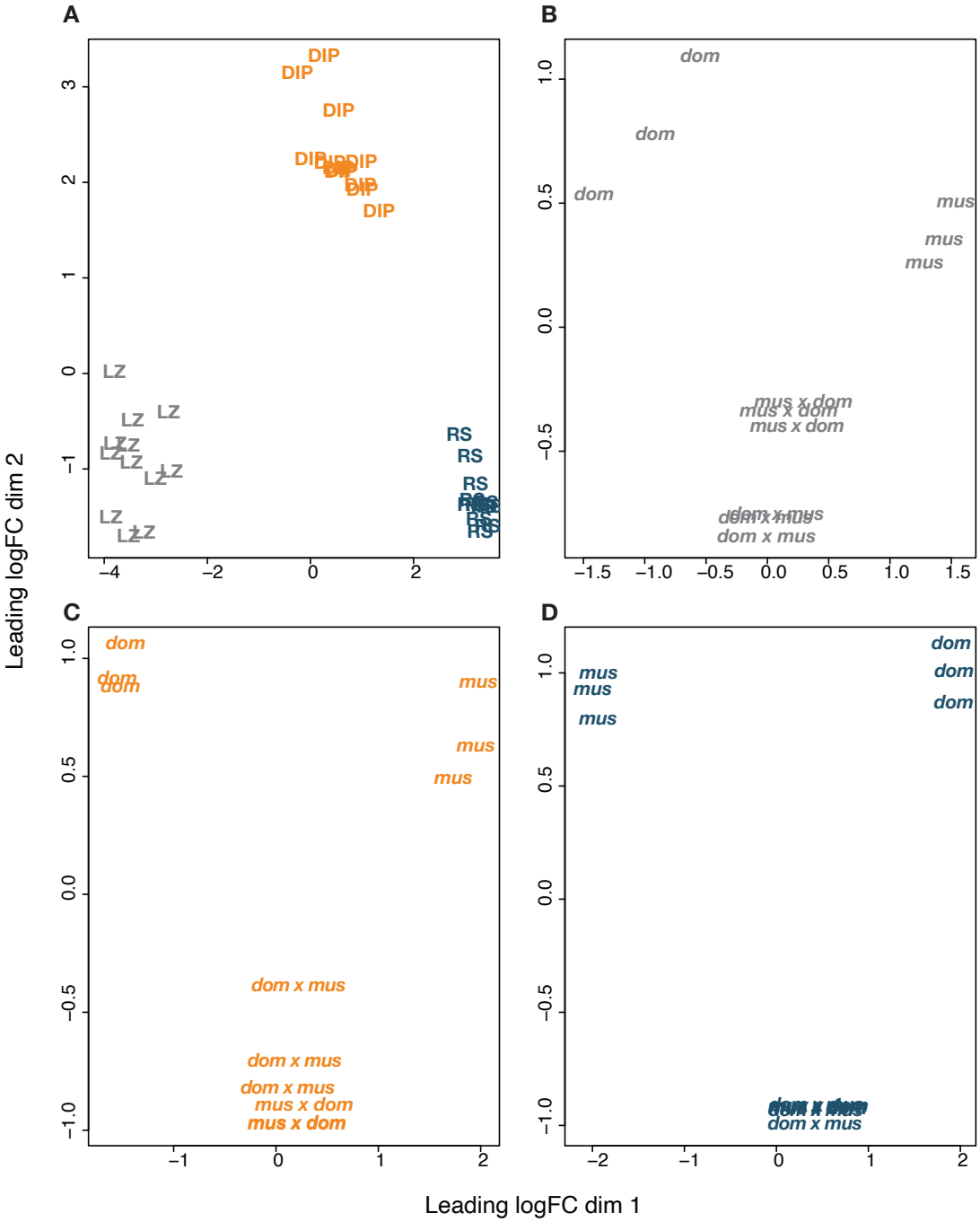

Figure S1. Clustering of gene expression profiles. Multidimensional scaling plots (MDS) of the Euclidean distance among gene expression profiles. Distance approximates the typical log2 fold changes between samples. **A)** RNAseq profiles cluster overall by cell type. LZ = leptotene/zygotene cells (gray), DIP = diplotene cells (orange), RS = round spermatids (blue). **B-D)** Within each cell type, RNAseq profiles cluster by subspecies, with F1 hybrids intermediate to the two parental subspecies. **B)** LZ = leptotene/zygotene cells (gray). **C)** DIP = diplotene cells (orange). **D)** RS = round spermatids (blue)

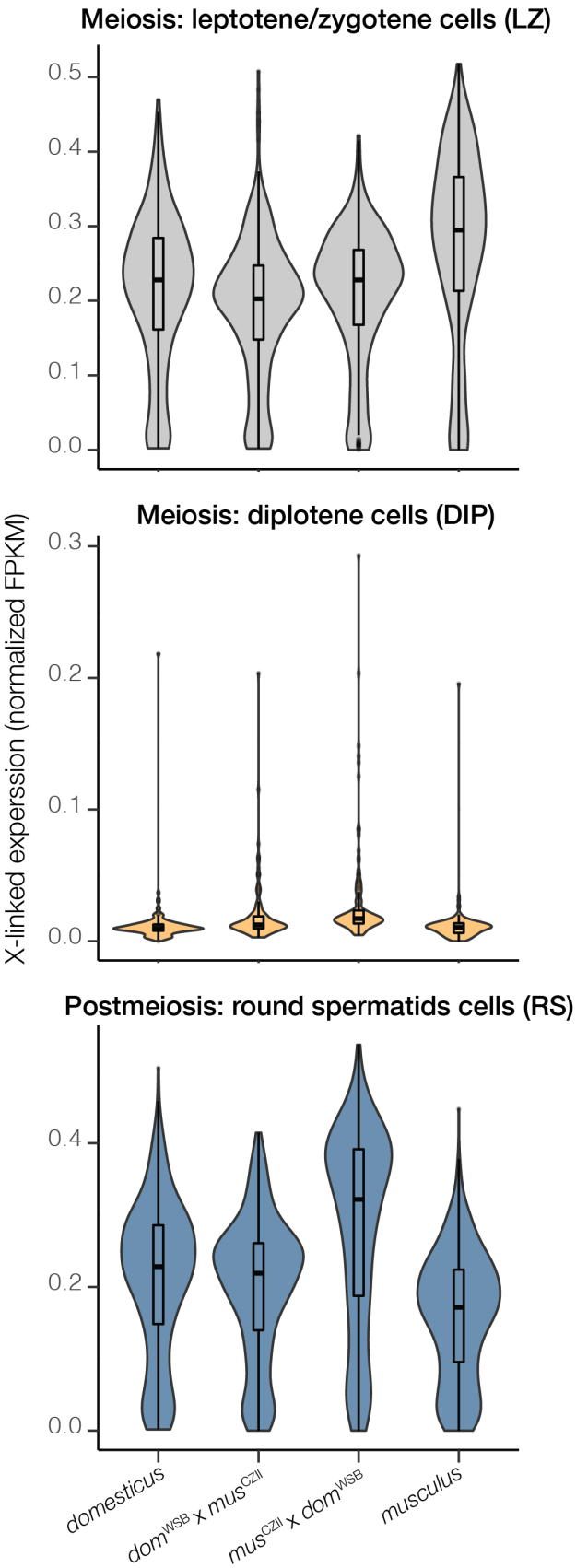

722

FigS2. X chromosome expression across different cell types and crosses. The distribution of X-linked gene expression in normalized FPKM values (values range 0 to 1). The violin plots show the density of genes with a given expression level and the boxplots depict the median values and quartiles. Gene expression was restricted to genes that have an FPKM > 1 in at least 3 samples per cell type. X-linked expression was elevated in diplotene cells of both hybrids and in round spermatids of ♀ *mus*^{CZII} × ♂ *dom*^{WSB} hybrids.

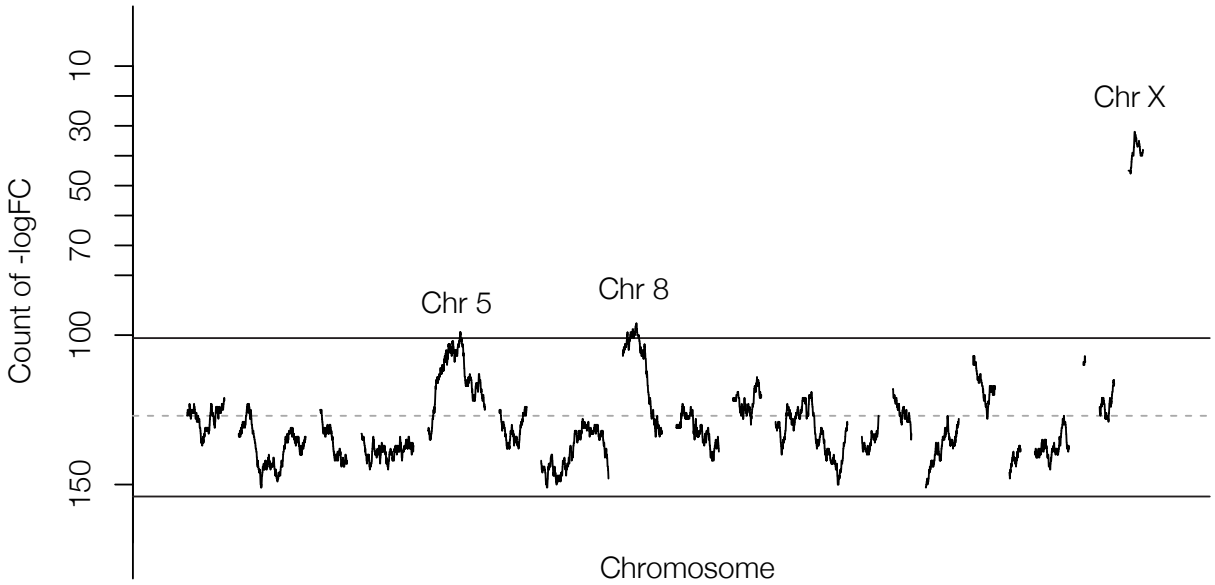

Figure S3. Spatial patterns of postmeiotic expression between subfertile hybrids. Sliding-gene windows (250 genes) for counts of underexpressed genes in postmeiotic cells (round spermatids) between ♀ *mus*^{CZII} × ♂ *dom*^{WSB} hybrids and ♀ *dom*^{WSB} x ♂ *mus*^{CZII} hybrids. Solid lines represent the 99th quantile modeled with a Poisson distribution. Note the Y-axis is plotted so that underexpressed genes fall below the 99th quantile and overexpressed genes are above the 99th quantile. Chromosomes 5 and 8 had relatively small windows of genes overexpressed in *Sly*-deficient ♀ *mus*^{CZII} × ♂ *dom*^{WSB} hybrids, but these windows did not coincide with known multicopy gene families (*Speer/α-takusan*).

REFERENCES

Alibert, P., F. Fel-Clair, K. Manolakou, J. Britton-Davidian, and J.-C. Auffray, 1997 Developmental stability, fitness, and trait size in laboratory hybrids between European subspecies of the house mouse. Evolution 51: 1284–1295.

Baker, C. L., S. Kajita, M. Walker, R. L. Saxl, N. Raghupathy *et al.*, 2015 PRDM9 drives evolutionary erosion of hotspots in *Mus musculus* through haplotype-specific initiation of meiotic recombination. PLoS Genet. 11: e1004916.

Balcova, M., B. Faltusova, V. Gergelits, T. Bhattacharyya, O. Mihola *et al.*, 2016 Hybrid sterility locus on chromosome X controls meiotic recombination rate in mouse. PLoS Genet. 12: e1005906.

Bank, C., R. Bürger, and J. Hermisson, 2012 The limits to parapatric speciation: Dobzhansky-Muller incompatibilities in a continent-island model. Genetics 191: 845–863.

Bateson, W., 1909 Heredity and variation in modern lights, pp. 85–101 in *Darwin and Modern Science*, edited by A. C. Seward. Cambridge University Press, Cambridge, UK.

Baudat, F., J. Buard, C. Grey, A. Fledel-Alon, C. Ober *et al.*, 2010 PRDM9 is a major determinant of meiotic recombination hotspots in humans and mice. Science 327: 836–840.

Benjamini, Y., and Y. Hochberg, 1995 Controlling the false discovery rate: a practical and powerful approach to multiple testing. J. R. Stat. Soc. Series B Stat. Methodol. 57: 289–300.

Bhattacharyya, T., S. Gregorova, O. Mihola, M. Anger, J. Sebestova *et al.*, 2013 Mechanistic basis of infertility of mouse intersubspecific hybrids. Proc. Natl. Acad. Sci. U. S. A. 110: E468–77.

Bhattacharyya, T., R. Reifova, S. Gregorova, P. Simecek, V. Gergelits *et al.*, 2014 X chromosome control of meiotic chromosome synapsis in mouse inter-subspecific hybrids. PLoS Genet. 10: e1004088.

Bímová, B. V., M. Macholán, S. J. E. Baird, P. Munclinger, P. Dufková *et al.*, 2011 Reinforcement selection acting on the European house mouse hybrid zone. Mol. Ecol. 20: 2403–2424.

Bolger, A. M., M. Lohse, and B. Usadel, 2014 Trimmomatic: a flexible trimmer for Illumina sequence data. Bioinformatics 30: 2114–2120.

Bracewell, R. R., B. J. Bentz, B. T. Sullivan, and J. M. Good, 2017 Rapid neo-sex chromosome evolution and incipient speciation in a major forest pest. Nat. Commun. 8: 1593.

Britton-Davidian, J., F. Fel-Clair, J. Lopez, P. Alibert, and P. Boursot, 2005 Postzygotic isolation between the two European subspecies of the house mouse: estimates from fertility. Biol. J. Linn. Soc. Lond. 84: 379–393.

Broad Institute, 2019 *Picard Tools*.

Buard, J., E. Rivals, D. Dunoyer de Segonzac, C. Garres, P. Caminade *et al.*, 2014 Diversity of Prdm9 zinc finger array in wild mice unravels new facets of the evolutionary turnover of this coding minisatellite. PLoS One 9: e85021.

Campbell, P., J. M. Good, and M. W. Nachman, 2013 Meiotic sex chromosome inactivation is disrupted in sterile hybrid male house mice. Genetics 193: 819–828.

Campbell, P., and M. W. Nachman, 2014 X–Y interactions underlie sperm head abnormality in hybrid male house mice. Genetics 196: 1231–1240.

Case, A. L., F. R. Finseth, C. M. Barr, and L. Fishman, 2016 Selfish evolution of cytonuclear hybrid incompatibility in *Mimulus*. Proc. Biol. Sci. 283: 20161493.

Cocquet, J., P. J. I. Ellis, S. K. Mahadevaiah, N. A. Affara, D. Vaiman *et al.*, 2012 A genetic basis for a postmeiotic X versus Y chromosome intragenomic conflict in the mouse. PLoS Genet. 8: e1002900.

792 Cocquet, J., P. J. I. Ellis, Y. Yamauchi, S. K. Mahadevaiah, N. A. Affara *et al.*, 2009 The
793 multicopy gene Sly represses the sex chromosomes in the male mouse germline after
794 meiosis. PLoS Biol. 7: e1000244.
795 Cocquet, J., P. J. I. Ellis, Y. Yamauchi, J. M. Riel, T. P. S. Karacs *et al.*, 2010 Deficiency in the
796 multicopy Sycp3-like X-linked genes Slx and Slxl1 causes major defects in spermatid
797 differentiation. Mol. Biol. Cell 21: 3497–3505.
798 Coughlan, J. M., and D. R. Matute, 2020 The importance of intrinsic postzygotic barriers
799 throughout the speciation process. Philos. Trans. R. Soc. Lond. B Biol. Sci. 375: 20190533.
800 Cutter, A. D., 2012 The polymorphic prelude to Bateson-Dobzhansky-Muller incompatibilities.
801 Trends Ecol. Evol. 27: 209–218.
802 Cutter, A. D., and J. D. Bundus, 2020 Speciation and the developmental alarm clock. Elife 9:
803 e56276.
804 Davies, B., E. Hatton, N. Altemose, J. G. Hussin, F. Pratto *et al.*, 2016 Re-engineering the zinc
805 fingers of PRDM9 reverses hybrid sterility in mice. Nature 530: 171–176.
806 Dobzhansky, T., 1937 *Genetics and the Origin of Species*. Columbia University Press.
807 Dufková, P., M. Macholán, and J. Piálek, 2011 Inference of selection and stochastic effects in
808 the house mouse hybrid zone. Evolution 65: 993–1010.
809 Dumont, B. L., and B. A. Payseur, 2011 Genetic analysis of genome-scale recombination rate
810 evolution in house mice. PLoS Genet. 7: e1002116.
811 Ďureje, Ľ., M. Macholán, S. J. E. Baird, and J. Piálek, 2012 The mouse hybrid zone in Central
812 Europe: from morphology to molecules. J. Vertebr. Biol. 61: 308–318.
813 Duvaux, L., K. Belkhir, M. Boulesteix, and P. Boursot, 2011 Isolation and gene flow: inferring the
814 speciation history of European house mice. Mol. Ecol. 20: 5248–5264.
815 Dzur-Gejdosova, M., P. Simecek, S. Gregorova, T. Bhattacharyya, and J. Forejt, 2012
816 Dissecting the genetic architecture of F1 hybrid sterility in house mice. Evolution 66: 3321–
817 3335.
818 Ellis, P. J. I., J. Bacon, and N. A. Affara, 2011 Association of Sly with sex-linked gene
819 amplification during mouse evolution: a side effect of genomic conflict in spermatids? Hum.
820 Mol. Genet. 20: 3010–3021.
821 Flachs, P., T. Bhattacharyya, O. Mihola, J. Piálek, J. Forejt *et al.*, 2014 Prdm9 incompatibility
822 controls oligospermia and delayed fertility but no selfish transmission in mouse
823 intersubspecific hybrids. PLoS One 9: e95806.
824 Flachs, P., O. Mihola, P. Simeček, S. Gregorová, J. C. Schimenti *et al.*, 2012 Interallelic and
825 intergenic incompatibilities of the Prdm9 (Hst1) gene in mouse hybrid sterility. PLoS Genet.
826 8: e1003044.
827 Forejt, J., P. Jansa, and E. Parvanov, 2021 Hybrid sterility genes in mice (*Mus musculus*): a
828 peculiar case of PRDM9 incompatibility. Trends Genet.
829 Geraldes, A., P. Basset, K. L. Smith, and M. W. Nachman, 2011 Higher differentiation among
830 subspecies of the house mouse (*Mus musculus*) in genomic regions with low
831 recombination. Mol. Ecol. 20: 4722–4736.
832 Getun, I. V., B. Torres, and P. R. J. Bois, 2011 Flow cytometry purification of mouse meiotic
833 cells. J. Vis. Exp. 50: e2602.
834 Good, J. M., 2012 The conflict within and the escalating war between the sex chromosomes.
835 PLoS Genet. 8: e1002955.
836 Good, J. M., M. D. Dean, and M. W. Nachman, 2008a A complex genetic basis to X-linked
837 hybrid male sterility between two species of house mice. Genetics 179: 2213–2228.
838 Good, J. M., T. Giger, M. D. Dean, and M. W. Nachman, 2010 Widespread over-expression of
839 the X chromosome in sterile F1 hybrid mice. PLoS Genet. 6: e1001148.

Good, J. M., M. A. Handel, and M. W. Nachman, 2008b Asymmetry and polymorphism of hybrid male sterility during the early stages of speciation in house mice. Evolution 62: 50–65.

Green, C. D., Q. Ma, G. L. Manske, A. N. Shami, X. Zheng *et al.*, 2018 A comprehensive roadmap of murine spermatogenesis defined by single-cell RNA-Seq. Dev. Cell 46: 651–667.e10.

Gregorova, S., V. Gergelits, I. Chvatalova, T. Bhattacharyya, B. Valiskova *et al.*, 2018 Modulation of Prdm9-controlled meiotic chromosome asynapsis overrides hybrid sterility in mice. Elife 7: e34282.

Huang, S., J. Holt, C.-Y. Kao, L. McMillan, and W. Wang, 2014 A novel multi-alignment pipeline for high-throughput sequencing data. Database 2014.:

Hunnicutt, K. E., J. M. Good, and E. L. Larson, 2021 Unraveling patterns of disrupted gene expression across a complex tissue. bioRxiv 2021.07.08.451646.

Janoušek, V., L. Wang, K. Luzynski, P. Dufková, M. M. Vyskočilová *et al.*, 2012 Genome-wide architecture of reproductive isolation in a naturally occurring hybrid zone between *Mus musculus musculus* and *M. m. domesticus*. Mol. Ecol. 21: 3032–3047.

Katoh, K., and D. M. Standley, 2013 MAFFT multiple sequence alignment software version 7: improvements in performance and usability. Mol. Biol. Evol. 30: 772–780.

Kim, D., G. Pertea, C. Trapnell, H. Pimentel, R. Kelley *et al.*, 2013 TopHat2: accurate alignment of transcriptomes in the presence of insertions, deletions and gene fusions. Genome Biol. 14: R36.

Kono, H., M. Tamura, N. Osada, H. Suzuki, K. Abe *et al.*, 2014 Prdm9 polymorphism unveils mouse evolutionary tracks. DNA Res. 21: 315–326.

Kruger, A. N., M. A. Brogley, J. L. Huizinga, J. M. Kidd, D. G. de Rooij *et al.*, 2019 A neofunctionalized X-Linked ampliconic gene family is essential for male fertility and equal sex ratio in mice. Curr. Biol. 29: 3699–3706.e5.

Larson, E. L., S. Keeble, D. Vanderpool, M. D. Dean, and J. M. Good, 2017 The composite regulatory basis of the large X-effect in mouse speciation. Mol. Biol. Evol. 34: 282–295.

Larson, E. L., E. E. K. Kopania, and J. M. Good, 2018a Spermatogenesis and the evolution of mammalian sex chromosomes. Trends Genet. 34: 722–732.

Larson, E. L., D. Vanderpool, S. Keeble, M. Zhou, B. A. J. Sarver *et al.*, 2016 Contrasting levels of molecular evolution on the mouse X chromosome. Genetics 203: 1841–1857.

Larson, E. L., D. Vanderpool, B. A. J. Sarver, C. Callahan, S. Keeble *et al.*, 2018b The evolution of polymorphic hybrid incompatibilities in house mice. Genetics 209: 845–859.

Liao, Y., G. K. Smyth, and W. Shi, 2014 featureCounts: an efficient general purpose program for assigning sequence reads to genomic features. Bioinformatics 30: 923–930.

Li, H., and R. Durbin, 2009 Fast and accurate short read alignment with Burrows-Wheeler transform. Bioinformatics 25: 1754–1760.

Lindtke, D., and C. A. Buerkle, 2015 The genetic architecture of hybrid incompatibilities and their effect on barriers to introgression in secondary contact. Evolution 69: 1987–2004.

Loire, E., S. Tusso, P. Caminade, D. Severac, P. Boursot *et al.*, 2017 Do changes in gene expression contribute to sexual isolation and reinforcement in the house mouse? Mol. Ecol. 26: 5189–5202.

Lustyk, D., S. Kinský, K. K. Ullrich, M. Yancoskie, L. Kašíková *et al.*, 2019 Genomic structure of Hstx2 modifier of Prdm9-dependent hybrid male sterility in mice. Genetics 213: 1047–1063.

Macholán, M., S. J. E. Baird, P. Dufková, P. Munclinger, B. V. Bímová *et al.*, 2011 Assessing multilocus introgression patterns: a case study on the mouse X chromosome in central Europe. Evolution 65: 1428–1446.

887 Macholán, M., S. J. E. Baird, A. Fornůsková, I. Martincová, P. Rubík *et al.*, 2019 Widespread
888 introgression of the *Mus musculus musculus* Y chromosome in Central Europe. bioRxiv
889 2019.12.23.887471.
890 Macholán, M., S. J. E. Baird, P. Munclinger, P. Dufková, B. Bímová *et al.*, 2008 Genetic conflict
891 outweighs heterogametic incompatibility in the mouse hybrid zone? BMC Evol. Biol. 8: 271.
892 Macholán, M., S. J. E. Baird, J. Piálek, and P. Munclinger, 2012 *Evolution of the House Mouse*.
893 Cambridge University Press.
894 Macholán, M., P. Munclinger, M. Sugerková, P. Dufková, B. Bímová *et al.*, 2007 Genetic
895 analysis of autosomal and X-linked markers across a mouse hybrid zone. Evolution 61:
896 746–771.
897 Mack, K. L., P. Campbell, and M. W. Nachman, 2016 Gene regulation and speciation in house
898 mice. Genome Res. 26: 451–461.
899 Mandeville, E. G., T. L. Parchman, K. G. Thompson, R. I. Compton, K. R. Gelwicks *et al.*, 2017
900 Inconsistent reproductive isolation revealed by interactions between Catostomus fish
901 species. Evol Lett 1: 255–268.
902 Margolin, G., P. P. Khil, J. Kim, M. A. Bellani, and R. D. Camerini-Otero, 2014 Integrated
903 transcriptome analysis of mouse spermatogenesis. BMC Genomics 15: 39.
904 Martincová, I., Ľ. Ďureje, S. J. E. Baird, and J. Piálek, 2019a Sperm quality parameters are
905 increased and asymmetric in house mouse hybrids. bioRxiv 666511.
906 Martincová, I., Ľ. Ďureje, J. Kreisinger, M. Macholán, and J. Piálek, 2019b Phenotypic effects of
907 the Y chromosome are variable and structured in hybrids among house mouse recombinant
908 lines. Ecol. Evol. 9: 6124–6137.
909 McCarthy, D. J., Y. Chen, and G. K. Smyth, 2012 Differential expression analysis of multifactor
910 RNA-Seq experiments with respect to biological variation. Nucleic Acids Res. 40: 4288–
911 4297.
912 Meiklejohn, C. D., E. L. Landeen, K. E. Gordon, T. Rzatkiewicz, S. B. Kingan *et al.*, 2018 Gene
913 flow mediates the role of sex chromosome meiotic drive during complex speciation. Elife 7:
914 e35468.
915 Mihola, O., Z. Trachtulec, C. Vlcek, J. C. Schimenti, and J. Forejt, 2009 A mouse speciation
916 gene encodes a meiotic histone H3 methyltransferase. Science 323: 373–375.
917 Mistry, J., S. Chuguransky, L. Williams, M. Qureshi, G. A. Salazar *et al.*, 2021 Pfam: The protein
918 families database in 2021. Nucleic Acids Res. 49: D412–D419.
919 Moretti, C., M. Blanco, C. Ialy-Radio, M.-E. Serrentino, C. Gobé *et al.*, 2020 Battle of the sex
920 chromosomes: competition between X and Y chromosome-encoded proteins for partner
921 interaction and chromatin occupancy drives multicopy gene expression and evolution in
922 Muroid rodents. Mol. Biol. Evol. 37: 3453–3468.
923 Moretti, C., M.-E. Serrentino, C. Ialy-Radio, M. Delessard, T. A. Soboleva *et al.*, 2017 SLY
924 regulates genes involved in chromatin remodeling and interacts with TBL1XR1 during
925 sperm differentiation. Cell Death Differ. 24: 1029–1044.
926 Morgan, K., B. Harr, M. A. White, B. A. Payseur, and L. M. Turner, 2020 Disrupted gene
927 networks in subfertile hybrid house mice. Mol. Biol. Evol. 37: 1547–1562.
928 Morgan, A. P., and F. Pardo-Manuel de Villena, 2017 Sequence and structural diversity of
929 mouse Y chromosomes. Mol. Biol. Evol. 34: 3186–3204.
930 Moyle, L. C., and T. Nakazato, 2010 Hybrid incompatibility “snowballs” between Solanum
931 species. Science 329: 1521–1523.
932 Mueller, J. L., S. K. Mahadevaiah, P. J. Park, P. E. Warburton, D. C. Page *et al.*, 2008 The
933 mouse X chromosome is enriched for multicopy testis genes showing postmeiotic
934 expression. Nat. Genet. 40: 794–799.

Mueller, J. L., H. Skaletsky, L. G. Brown, S. Zaghlul, S. Rock *et al.*, 2013 Independent specialization of the human and mouse X chromosomes for the male germ line. Nat. Genet. 45: 1083–1087.

Mukaj, A., J. Piálek, V. Fotopulosova, A. P. Morgan, L. Odenthal-Hesse *et al.*, 2020 Prdm9 intersubspecific interactions in hybrid male sterility of house mouse. Mol. Biol. Evol. 37: 3423–3438.

Muller, H., 1942 Isolating mechanisms, evolution, and temperature. Biol. Symp. 6: 71–125.

Myers, S., R. Bowden, A. Tumian, R. E. Bontrop, C. Freeman *et al.*, 2010 Drive against hotspot motifs in primates implicates the PRDM9 gene in meiotic recombination. Science 327: 876–879.

Oka, A., T. Aoto, Y. Totsuka, R. Takahashi, M. Ueda *et al.*, 2007 Disruption of genetic interaction between two autosomal regions and the X chromosome causes reproductive isolation between mouse strains derived from different subspecies. Genetics 175: 185–197.

Oka, A., A. Mita, N. Sakurai-Yamatani, H. Yamamoto, N. Takagi *et al.*, 2004 Hybrid breakdown caused by substitution of the X chromosome between two mouse subspecies. Genetics 166: 913–924.

Oliver, P. L., L. Goodstadt, J. J. Bayes, Z. Birtle, K. C. Roach *et al.*, 2009 Accelerated evolution of the Prdm9 speciation gene across diverse metazoan taxa. PLoS Genet. 5: e1000753.

Parvanov, E. D., P. M. Petkov, and K. Paigen, 2010 Prdm9 controls activation of mammalian recombination hotspots. Science 327: 835.

Payseur, B. A., J. G. Krenz, and M. W. Nachman, 2004 Differential patterns of introgression across the X chromosome in a hybrid zone between two species of house mice. Evolution 58: 2064–2078.

Pedersen, B. S., and A. R. Quinlan, 2018 Mosdepth: quick coverage calculation for genomes and exomes. Bioinformatics 34: 867–868.

Phifer-Rixey, M., B. Harr, and J. Hey, 2020 Further resolution of the house mouse (Mus musculus) phylogeny by integration over isolation-with-migration histories. BMC Evol. Biol. 20: 120.

Phifer-Rixey, M., and M. W. Nachman, 2015 Insights into mammalian biology from the wild house mouse *Mus musculus*. Elife 4: e05959.

Rathje, C. C., E. E. P. Johnson, D. Drage, C. Patinioti, G. Silvestri *et al.*, 2019 Differential sperm motility mediates the sex ratio drive shaping mouse sex chromosome evolution. Curr. Biol. 29: 3692–3698.e4.

R Core Team, 2020 *R: A language and environment for statistical computing*. R Foundation for Statistical Computing, Vienna, Austria.

Reed, L. K., and T. A. Markow, 2004 Early events in speciation: polymorphism for hybrid male sterility in Drosophila. Proc. Natl. Acad. Sci. U. S. A. 101: 9009–9012.

Robinson, M. D., D. J. McCarthy, and G. K. Smyth, 2010 edgeR: a Bioconductor package for differential expression analysis of digital gene expression data. Bioinformatics 26: 139–140.

Schwahn, D. J., R. J. Wang, M. A. White, and B. A. Payseur, 2018 Genetic dissection of hybrid male sterility across stages of spermatogenesis. Genetics 210: 1453–1465.

Smadja, C., and G. Ganem, 2007 Divergence of odorant signals within and between the two European subspecies of the house mouse. Behav. Ecol. 19: 223–230.

Smadja, C., and G. Ganem, 2002 Subspecies recognition in the house mouse: a study of two populations from the border of a hybrid zone. Behav. Ecol. 13: 312–320.

Smagulova, F., K. Brick, Y. Pu, R. D. Camerini-Otero, and G. V. Petukhova, 2016 The evolutionary turnover of recombination hot spots contributes to speciation in mice. Genes Dev. 30: 266–280.

Soh, Y. Q. S., J. Alföldi, T. Pyntikova, L. G. Brown, T. Graves *et al.*, 2014 Sequencing the mouse Y chromosome reveals convergent gene acquisition and amplification on both sex chromosomes. Cell 159: 800–813.

Storchová, R., S. Gregorová, D. Buckiová, V. Kyselová, P. Divina *et al.*, 2004 Genetic analysis of X-linked hybrid sterility in the house mouse. Mamm. Genome 15: 515–524.

Suzuki, T. A., and M. W. Nachman, 2015 Speciation and reduced hybrid female fertility in house mice. Evolution 69: 2468–2481.

Sweigart, A. L., and L. E. Flagel, 2015 Evidence of natural selection acting on a polymorphic hybrid incompatibility locus in *Mimulus*. Genetics 199: 543–554.

Teeter, K. C., L. M. Thibodeau, Z. Gompert, C. A. Buerkle, M. W. Nachman *et al.*, 2010 The variable genomic architecture of isolation between hybridizing species of house mice. Evolution 64: 472–485.

Tucker, P. K., R. D. Sage, J. Warner, A. C. Wilson, and E. M. Eicher, 1992 Abrupt cline for sex chromosomes in a hybrid zone between two species of mice. Evolution 46: 1146–1163.

Turner, J. M. A., 2015 Meiotic silencing in mammals. Annu. Rev. Genet. 49: 395–412.

Turner, L. M., and B. Harr, 2014 Genome-wide mapping in a house mouse hybrid zone reveals hybrid sterility loci and Dobzhansky-Muller interactions. Elife 3: e02504.

Turner, L. M., D. J. Schwahn, and B. Harr, 2012 Reduced male fertility is common but highly variable in form and severity in a natural house mouse hybrid zone. Evolution 66: 443–458.

Turner, L. M., M. A. White, D. Tautz, and B. A. Payseur, 2014 Genomic networks of hybrid sterility. PLoS Genet. 10: e1004162.

Vanlerberghe, F., B. Dod, P. Boursot, M. Bellis, and F. Bonhomme, 1986 Absence of Y-chromosome introgression across the hybrid zone between *Mus musculus domesticus* and *Mus musculus musculus*. Genet. Res. 48: 191–197.

Vara, C., L. Capilla, L. Ferretti, A. Ledda, R. A. Sánchez-Guillén *et al.*, 2019 PRDM9 diversity at fine geographical scale reveals contrasting evolutionary patterns and functional constraints in natural populations of house mice. Mol. Biol. Evol. 36: 1686–1700.

Vegesna, R., M. Tomaszkiewicz, P. Medvedev, and K. D. Makova, 2019 Dosage regulation, and variation in gene expression and copy number of human Y chromosome ampliconic genes. PLoS Genet. 15: e1008369.

Vyskočilová, M., Z. Trachtulec, J. Forejt, and J. Piálek, 2005 Does geography matter in hybrid sterility in house mice? Biol. J. Linn. Soc. Lond. 84: 663–674.

Wang, R. J., C. Ané, and B. A. Payseur, 2013 The evolution of hybrid incompatibilities along a phylogeny. Evolution 67: 2905–2922.

White, M. A., B. Steffy, T. Wiltshire, and B. A. Payseur, 2011 Genetic dissection of a key reproductive barrier between nascent species of house mice. Genetics 189: 289–304.

Widmayer, S. J., M. A. Handel, and D. L. Aylor, 2020 Age and genetic background modify hybrid male sterility in house mice. Genetics 216: 585–597.

Yang, H., J. R. Wang, J. P. Didion, R. J. Buus, T. A. Bell *et al.*, 2011 Subspecific origin and haplotype diversity in the laboratory mouse. Nat. Genet. 43: 648–655.

Yates, A. D., P. Achuthan, W. Akanni, J. Allen, J. Allen *et al.*, 2019 Ensembl 2020. Nucleic Acids Res. 48: D682–D688.

Zuellig, M. P., and A. L. Sweigart, 2018 A two-locus hybrid incompatibility is widespread, polymorphic, and active in natural populations of *Mimulus*. Evolution 72: 2394–2405.